



Electronic nematic correlations in the stress-free tetragonal state of $\text{BaFe}_{2-x}\text{Ni}_x\text{As}_2$

Haoran Man,¹ Xingye Lu,^{1,2,*} Justin S. Chen,¹ Rui Zhang,¹ Wenliang Zhang,² Huiqian Luo,² J. Kulda,³ A. Ivanov,³ T. Keller,^{4,5} Emilia Morosan,¹ Qimiao Si,¹ and Pengcheng Dai^{1,†}

¹Department of Physics and Astronomy, Rice University, Houston, Texas 77005, USA

²Beijing National Laboratory for Condensed Matter Physics, Institute of Physics, Chinese Academy of Sciences, Beijing 100190, China

³Institut Laue-Langevin, 6, rue Jules Horowitz, BP 156, 38042 Grenoble Cedex 9, France

⁴Max-Planck-Institut für Festkörperforschung, Heisenbergstrasse 1, D-70569 Stuttgart, Germany

⁵Max Planck Society Outstation at the Forschungsneutronenquelle Heinz Maier-Leibnitz (MLZ), D-85747 Garching, Germany

(Received 11 May 2015; published 22 October 2015)

We use transport and neutron scattering to study electronic, structural, and magnetic properties of the electron-doped $\text{BaFe}_{2-x}\text{Ni}_x\text{As}_2$ iron pnictides in uniaxial-strained and external-stress-free detwinned states. Using a specially designed *in situ* mechanical detwinning device, we demonstrate that the in-plane resistivity anisotropy observed in the uniaxial-strained tetragonal state of $\text{BaFe}_{2-x}\text{Ni}_x\text{As}_2$ below a temperature T^* , previously identified as a signature of the electronic nematic phase, is also present in the stress-free tetragonal phase below T^{**} ($< T^*$). By carrying out neutron scattering measurements on BaFe_2As_2 and $\text{BaFe}_{1.97}\text{Ni}_{0.03}\text{As}_2$, we argue that the resistivity anisotropy in the stress-free tetragonal state of iron pnictides arises from the magnetoelastic coupling associated with antiferromagnetic order. These results thus indicate that the local lattice distortion and nematic spin correlations are responsible for the resistivity anisotropy in the tetragonal state of stress-free iron pnictides, and suggest that resistivity anisotropy, spin excitation anisotropy, and orbital ordering found in the paramagnetic state of uniaxial-strained iron pnictides are due to the externally applied uniaxial strain via an enhanced nematic susceptibility.

DOI: [10.1103/PhysRevB.92.134521](https://doi.org/10.1103/PhysRevB.92.134521)

PACS number(s): 74.25.Ha, 74.25.Jb, 74.70.-b, 78.70.Nx

I. INTRODUCTION

There is growing experimental evidence suggesting that the electronic nematic phase, a translationally invariant metallic phase (satisfying the 90° -rotational or C_4 symmetry) with a spontaneously generated spatial electronic anisotropy, is intimately connected with high-transition-temperature (high- T_c) superconductivity [1]. For iron pnictide superconductors such as $\text{BaFe}_{2-x}\text{T}_x\text{As}_2$ ($T = \text{Co, Ni}$) [2–7], their parent compound BaFe_2As_2 exhibits a tetragonal to orthorhombic structural phase transition at temperature T_s , followed by a paramagnetic to antiferromagnetic (AF) phase transition at T_N ($T_s \geq T_N$) with a collinear AF structure [Fig. 1(a)] [5–7]. Upon electron-doping via Co or Ni substitution for Fe, the T_N and T_s are gradually suppressed and optimal superconductivity emerges near $x \approx 0.1$ for $\text{BaFe}_{2-x}\text{Ni}_x\text{As}_2$ [8–12]. Due to the formation of twin domains in the orthorhombic state of $\text{BaFe}_{2-x}\text{T}_x\text{As}_2$ below T_s , the intrinsic electronic properties of these materials can be probed by applying a uniaxial pressure (strain) along one axis of the orthorhombic lattice to detwin the single crystal [13–16]. While there is indeed a large in-plane resistivity anisotropy in the uniaxial-strained detwinned $\text{BaFe}_{2-x}\text{T}_x\text{As}_2$ below T_s and T_N due to the C_4 -symmetry-breaking collinear AF structure, the anisotropy persists in the paramagnetic tetragonal state below a characteristic temperature T^* ($T^* > T_s \geq T_N$), thus suggesting the presence of electronic nematic correlations above T_s and below T^* [13–18]. However, since the uniaxial strain necessary to detwin the sample also enhances T_N [19] and introduces an explicit symmetry-breaking field, it is unclear

whether there will be resistivity anisotropy in the stress-free tetragonal state below T^* upon releasing the applied external uniaxial strain as expected in an ideal electronic nematic phase. From transport [16–18], inelastic neutron scattering [20], and thermodynamic measurements [21], T^* is believed to mark a temperature range of nematic fluctuations with structure and magnetic phase transitions occurring at T_s and T_N , respectively. On the other hand, magnetic torque and x-ray diffraction experiments on supposedly strain-free samples of BaFe_2As_2 and $\text{BaFe}_2(\text{As}_{1-x}\text{P}_x)_2$ suggest that T^* is a signature of a “true” second-order nematic phase transition from the high-temperature tetragonal phase to a low-energy orthorhombic phase, and there are no additional C_4 -symmetry-breaking structural transitions below T^* [22]. Even in the AF-ordered phase, the effect of the uniaxial strain on the sample detwinning ratio and resistivity anisotropy is unclear. To understand the role of electronic nematic phase in high- T_c superconductivity, it is important to reveal the origin of resistivity anisotropy above T_s without external uniaxial strain and determine the nature of the nematic correlations below T^* [23]. By establishing uniaxial pressure dependence of the resistivity anisotropy below and above T_N , T_s , and T^* in $\text{BaFe}_{2-x}\text{T}_x\text{As}_2$, we can conclusively determine the effect of uniaxial strain on the resistivity in different phases, and separate uniaxial-strain-induced resistivity anisotropy from intrinsic electronic anisotropy in these materials.

We use transport and neutron scattering to study the resistivity anisotropy, magnetic order, and lattice distortion in parent compound BaFe_2As_2 ($T_N \approx T_s \approx 138$ K) and electron-doped $\text{BaFe}_{2-x}\text{Ni}_x\text{As}_2$ ($x = 0.015, 0.03, 0.05, 0.065$). In previous transport [13–18], neutron scattering [19,20], and angle-resolved photoemission spectroscopy (ARPES) [24,25] measurements, the applied uniaxial pressure necessary to detwin the crystal in the orthorhombic AF phase remains in the paramagnetic tetragonal state ($T > T_N, T_s$), thus

*Present address: Paul Scherrer Institut, Swiss Light Source, CH-5232 Villigen PSI, Switzerland.

†pdai@rice.edu

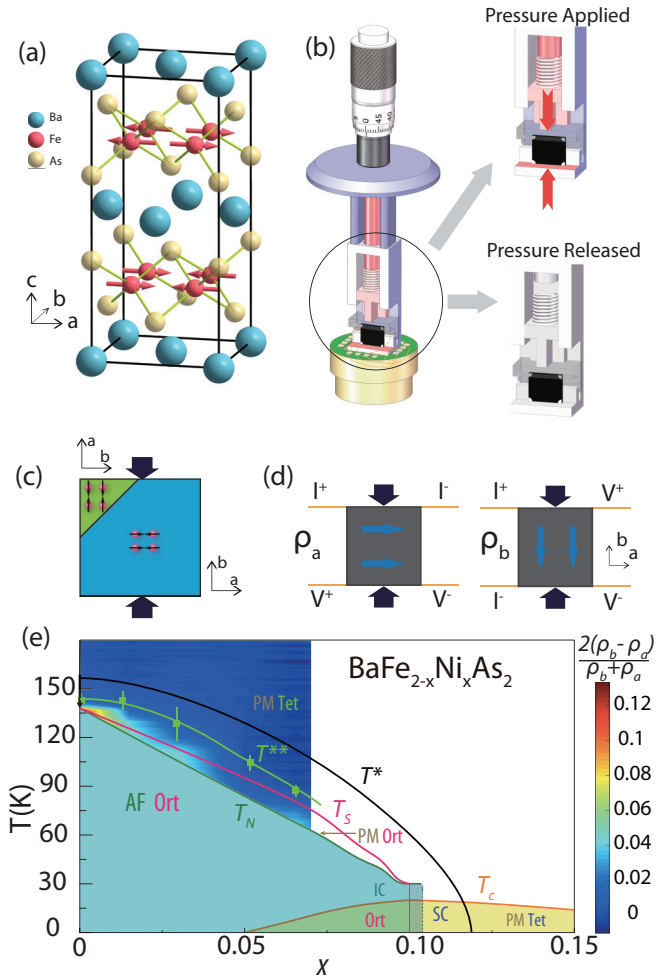


FIG. 1. (Color online) Summary of transport and neutron scattering results. (a) The crystal and magnetic structures of BaFe_{2-x}Ni_xAs₂ in the AF orthorhombic state where the arrows mark the moment directions of iron [6]. (b) Schematic diagram of the device used to change pressure on the sample *in situ*. A micrometer is used to adjust the length of the spring and therefore the pressure applied on the sample. The applied pressure then can be released by full retreat of the micrometer, as indicated in the expanded schematic on the right. (c) The uniaxial strain is applied along the *b* axis of the crystal, enlarging the blue domain and reducing the green domain. (d) Wire connection and current flow directions for resistivity measurements using Montgomery method. The black arrows indicate the uniaxial-pressure direction and the blue arrows in the sample are the current direction for each setup. (e) The electronic phase diagram of BaFe_{2-x}Ni_xAs₂ as a function of Ni doping as determined from previous experiments [12]. The spin excitation anisotropy temperatures under uniaxial strain are marked as T^* [20]. The AF orthorhombic (Ort), incommensurate AF (IC) [12], paramagnetic tetragonal (PM Tet), and superconductivity (SC) phases are clearly marked. T^{**} marks the temperature below which resistivity anisotropy appears in the strain-free tetragonal state.

complicating the interpretation of the observed in-plane resistivity and spin excitation anisotropy [13–20], as well as orbital ordering [24,25]. In addition, these devices cannot determine the uniaxial pressure dependence of the detwinning ratio in the AF-ordered phase, thus making it difficult to

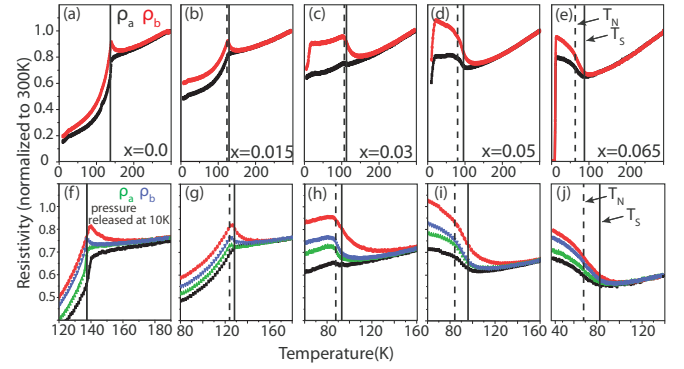


FIG. 2. (Color online) Temperature dependence of the resistivity anisotropy in strained and stress-free BaFe_{2-x}Ni_xAs₂. (a)–(e) Temperature dependence of the in-plane resistivity ρ_a (black) and ρ_b (red) under uniaxial strain for BaFe_{2-x}Ni_xAs₂ with $x = 0, 0.015, 0.03, 0.05, 0.065$, respectively. The vertical solid and dashed lines mark T_s and T_N , respectively, for these materials without uniaxial strain. (f)–(j) Expanded view of the data in (a)–(e). The green and blue data points are ρ_a and ρ_b resistivity obtained on warming after releasing the pressure at 10 K. In all cases, the resistivity is measured upon heating, with the same sample and same contacts (four-point Montgomery method; see Appendix for details).

reveal the intrinsic resistivity anisotropy in the AF-ordered and paramagnetic state of BaFe_{2-x}Ni_xAs₂. To avoid these problems, we have designed an *in situ* mechanical sample clamp which can apply and release uniaxial pressure at any temperature, similar to the device used to study the anisotropic optical response in iron pnictides [26]. Figure 1(b) shows the schematics of the sample stick with a micrometer on the top. The magnitude of the uniaxial pressure along the *b*-axis direction of the orthorhombic lattice is applied by a spring that is controlled by the displacement of the micrometer (and external applied pressure) [Fig. 1(c)]. By applying uniaxial pressure at room temperature (above T_N and T_s), cooling the sample to below T_N , and then releasing the pressure, we can in principle obtain the single-domain sample without external strain (stress free). We can also use this device to determine uniaxial pressure dependence of the resistivity anisotropy at any temperature, thus revealing whether uniaxial pressure can affect the transport properties of the ~100% detwinned AF-ordered iron pnictides.

To conclusively determine the sample detwinning ratio and compare it with the resistivity anisotropy measurement, we used two original sample sticks: one for transport in a physical property measurement system (PPMS) and one for a neutron scattering experiment on the IN8 triple-axis spectrometer at Institut Laue-Langevin (ILL), Grenoble, France. Our key finding is that the resistivity anisotropy in BaFe_{2-x}Ni_xAs₂ seen in the uniaxial-strained tetragonal phase below T^* is also present in the stress-free tetragonal state, but at a lower temperature $T^{**} < T^*$ [Fig. 1(e) and Fig. 2]. Although these results would naively suggest that resistivity anisotropy is an intrinsic property of the paramagnetic tetragonal phase of BaFe_{2-x}Ni_xAs₂ consistent with the presence of an ideal electronic nematic state [1], our neutron Larmor diffraction measurements using the three-axes spin echo spectrometer (TRISP) at Heinz Maier-Leibnitz, Garching, Germany [27–30]

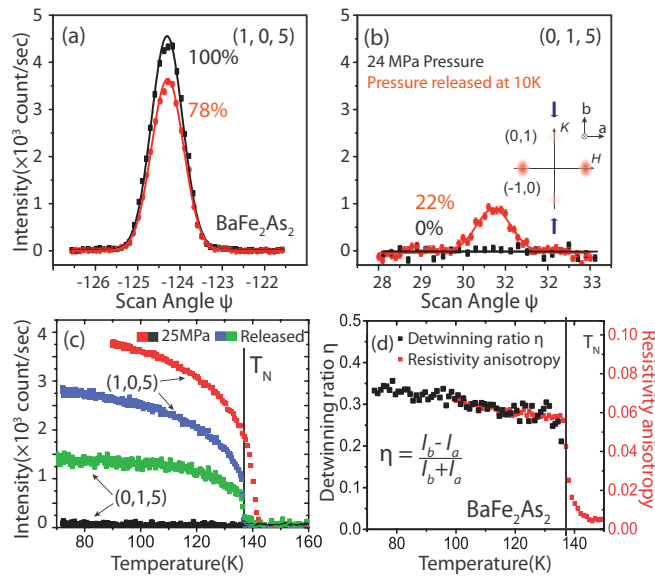


FIG. 3. (Color online) Temperature dependence of magnetic Bragg peaks at (1,0,5) and (0,1,5) in strained and stress-free BaFe_2As_2 . (a) Transverse scan through magnetic Bragg peak (1,0,5) with and without uniaxial strain at 10 K obtained using flat-cone setup and *in situ* sample clamp on IN8. (b) Identical scans through (0,1,5) peak on IN8. (c) Temperature dependence of the magnetic scattering at (1,0,5) and (0,1,5) in strained and stress-free case. (d) Estimated temperature dependence of the detwinning ratio η and resistivity anisotropy, defined as $2(\rho_b - \rho_a)/(\rho_b + \rho_a)$.

on temperature dependence of the lattice spacing (d) and its distortion (Δd) in lightly electron-doped iron pnictides reveal that the lattice distortion increases upon cooling, passes smoothly across T_s , and enhances dramatically on approaching T_N with no observable anomaly above T_s (Figs. 3 and 4). These results suggest that the resistivity anisotropy observed in the external uniaxial-pressure-free tetragonal state of $\text{BaFe}_{2-x}\text{Ni}_x\text{As}_2$ arises from a strong magnetoelastic coupling induced by AF order, and such anisotropy would vanish in a strain-free paramagnetic tetragonal phase. Furthermore, our data indicate no additional thermodynamic phase transitions above T_s , consistent with earlier work [21,31]. Therefore, the Ising-nematic correlations, a state with no magnetic long-range order (staggered magnetization $M = 0$) but with local broken- C_4 -symmetry lattice distortion [32–34], is the driving force for the observed resistivity anisotropy (Fig. 5) [23,32–34]. These results suggest that the resistivity anisotropy [13–18], spin excitation anisotropy [20], and orbital ordering seen by ARPES experiments [24,25] in the tetragonal phase of uniaxial-strained $\text{BaFe}_{2-x}\text{As}_2$ are due entirely to the externally applied uniaxial strain via an enhanced nematic susceptibility. Furthermore, in the paramagnetic phase above T_N and T_s , the magnitude of the resistivity anisotropy is proportional to the applied uniaxial strain below ~ 90 MPa, consistent with previous work (Fig. 6) [16–18]. In the AF-ordered state, the resistivity anisotropy is only approximately associated with uniaxial strain and detwinning ratio in the partially twinned state. Upon reaching the fully detwinned state for uniaxial pressure above ~ 20 MPa, the resistivity anisotropy gradually increases with increasing pressure and

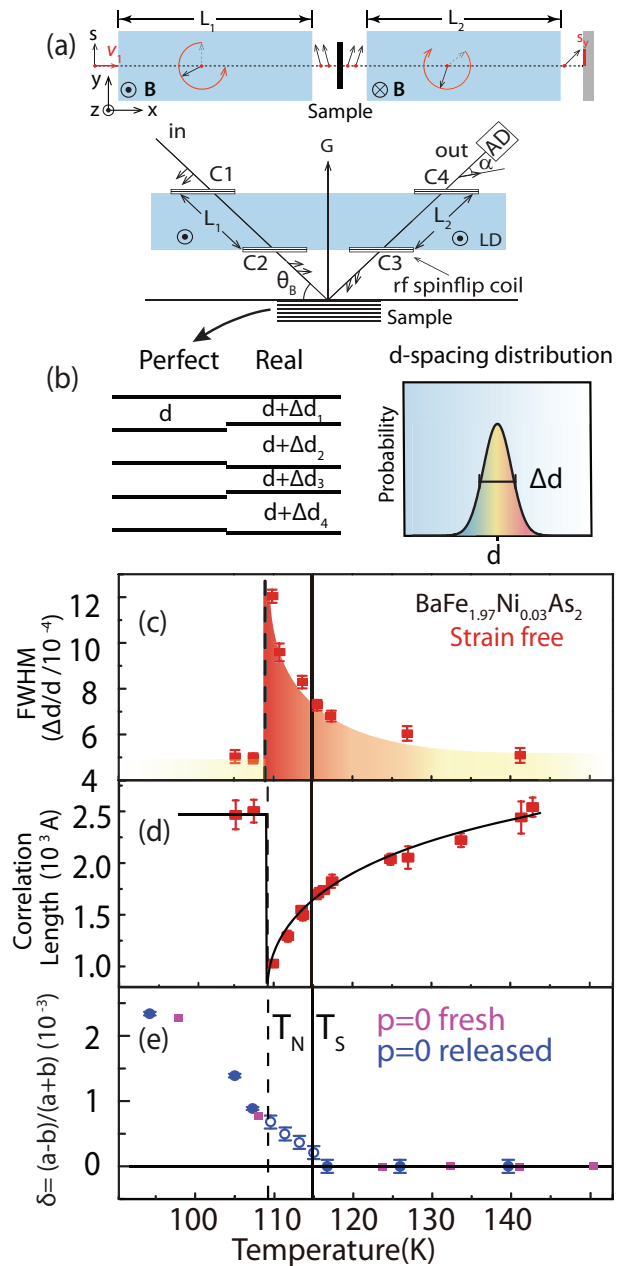


FIG. 4. (Color online) Schematic diagram of neutron Larmor diffraction setup and temperature dependence of the (4,0,0) Bragg peak d space and its distortion $\Delta d/d$. (a) Schematic diagram for the configuration of neutron Larmor diffraction measurements [27,29]. In neutron Larmor diffraction, the neutron precession directions are the same in L_1 and L_2 . The incident and diffracted neutrons also have the same velocity $v = v_1 = v_2$. (b) By measuring total neutron Larmor phase and its variation, one can accurately determine lattice spacing d and its distortion Δd . (c) Temperature dependence of the $\Delta d/d$ of $\text{BaFe}_{1.97}\text{Ni}_{0.03}\text{As}_2$ in full width at half maximum (FWHM). The solid and dashed vertical lines are T_s and T_N , respectively. There is no evidence for additional phase transition above T_s . (d) Temperature dependence of the lattice correlation length ξ as determined from neutron Larmor diffraction. (e) Temperature dependence of the estimated orthorhombicity δ for fresh and stress-free (first apply uniaxial pressure, then release pressure at low temperature) $\text{BaFe}_{1.97}\text{Ni}_{0.03}\text{As}_2$. The most dramatic changes in lattice distortion happen at T_N and not at T_s .

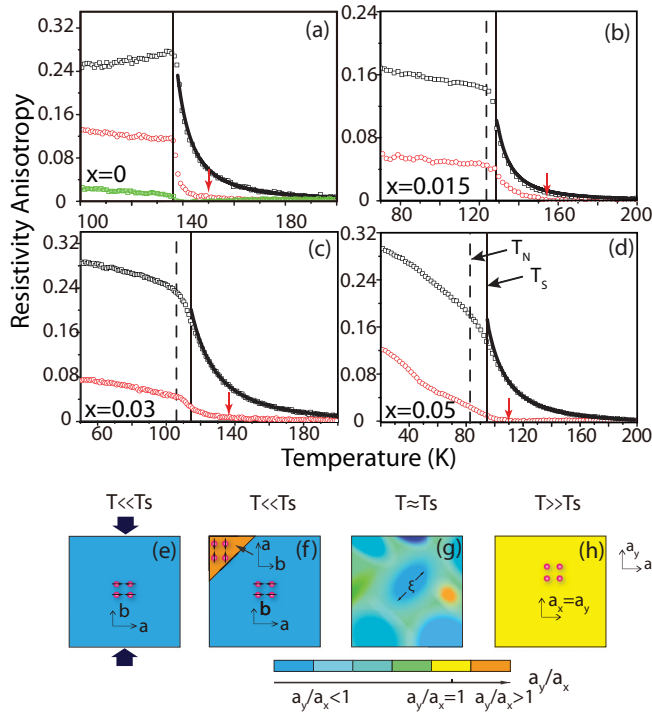


FIG. 5. (Color online) Temperature dependence of the in-plane resistivity anisotropy for strained and stress-free $\text{BaFe}_{2-x}\text{Ni}_x\text{As}_2$. (a)–(d) Temperature dependence of the in-plane resistivity anisotropy for $\text{BaFe}_{2-x}\text{Ni}_x\text{As}_2$ under uniaxial pressure (black) and pressure released at 10 K (red) on warming. Solid and dashed vertical lines mark T_s and T_N , respectively, for each Ni doping. The solid black line is a fit above T_s using Curie-Weiss functional form. The red arrows mark the estimated T^{**} . The green curve in (a) represents resistivity anisotropy measured upon cooling in the strain-free case (fresh sample) from room temperature. (e)–(h) Microscopic picture of what happens in the process of releasing uniaxial strain at low temperature. a and b are orthorhombic lattice parameters. At temperatures slightly above T_s in the stress-free case, the overall crystal structure is tetragonal but there are local orthorhombic lattice distortions induced by the strong magnetoelastic coupling, which gives rise to the observed resistivity anisotropy.

saturates for the pressure up to ~ 90 MPa. However, resistivity along (ρ_b , orthorhombic b -axis direction) and perpendicular (ρ_a , orthorhombic a -axis direction) to the uniaxial-pressure directions both decrease approximately linearly with increasing pressure, suggesting that transport properties of undoped iron pnictides can be affected by uniaxial strain even in the fully detwinned AF-ordered state (Fig. 6).

II. EXPERIMENTAL RESULTS

We first compare transport measurements obtained on single-domain samples detwinned using a standard mechanical clamp and the new device [Fig. 1(b)]. The resistivity data along the orthorhombic a and b directions are measured via the Montgomery method [35,36]. Resistivity ρ_a and ρ_b are measured in the same cycle using different current directions with the wiring diagram shown in Fig. 1(d) (see Appendix). Two sets of resistivity data as a function of temperature were collected for the detwinned crystals of $\text{BaFe}_{2-x}\text{Ni}_x\text{As}_2$.

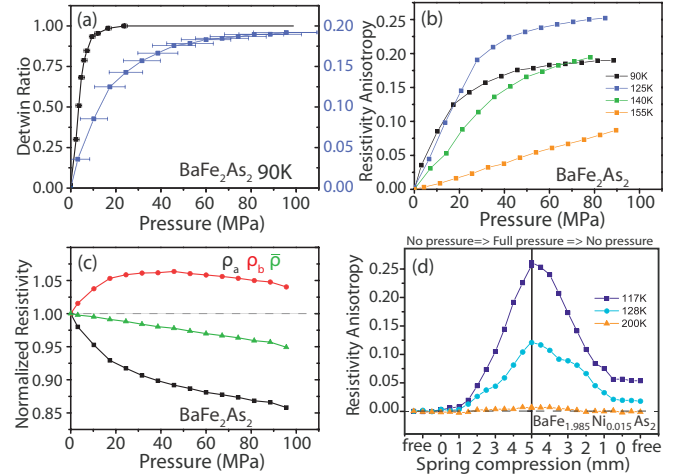


FIG. 6. (Color online) Comparison of uniaxial pressure dependence of detwinning ratio and resistivity anisotropy below and above T_N and T_s . Uniaxial pressure dependence of (a) resistivity anisotropy and detwinning ratio of BaFe_2As_2 at 90 K ($< T_N$); (b) resistivity anisotropy at 90 K, 129 K, 140 K, and 155 K; (c) resistivity along a and b axis direction at 90 K. (d) Uniaxial pressure dependence of resistivity anisotropy in $\text{BaFe}_{1.985}\text{Ni}_{0.015}\text{As}_2$ upon zero-pressure cooling and warming to different temperatures.

Figures 2(a)–2(e) show temperature dependence of ρ_a and ρ_b for $x = 0, 0.015, 0.03, 0.05, 0.065$, respectively, under ~ 10 MPa of uniaxial pressure. Consistent with previous work [15], we see clear resistivity anisotropy ($\rho_b > \rho_a$) at temperatures above the strain-free T_N and T_s marked as vertical dashed and solid lines, respectively. The green and blue lines in Figs. 2(f)–2(j) show ρ_a and ρ_b , respectively, on the warming cycle when the room-temperature applied strain is released at base temperature (10 K, stress-free state). The corresponding ρ_a and ρ_b under uniaxial strain in Figs. 2(a)–2(e) are shown as black and red lines in Figs. 2(f)–2(j).

In the undoped parent compound ($x = 0$), the uniaxial strain clearly increases the temperature below which the resistivity decreases with decreasing temperature [Fig. 2(f)], consistent with the notion that the uniaxial strain necessary for detwinning the sample also increases the T_N of the system [19]. In addition, we see that the uniaxial strain itself enhances the resistivity anisotropy both below and above T_N (T_s). Although much reduced, the resistivity anisotropy ($\rho_b > \rho_a$) is also present in the stress-free tetragonal state above T_N (T_s). When the Ni-doping level is increased to $x = 0.015, 0.03$, we find a similar trend for strained and stress-free resistivity [Figs. 2(g) and 2(h)]. Since T_N and T_s are now clearly separated, we can see that the resistivity reduction in the stress-free sample happens below T_N , and the resistivity anisotropy shows no observable anomaly across T_s . Upon further increasing the Ni-doping levels to $x = 0.05, 0.065$, the resistivity smoothly increases upon cooling across T_s and no longer displays a clear kink below T_N . At all doping levels studied, we find resistivity anisotropy in stress-free samples above T_N and T_s (Fig. 2).

Although transport data in Fig. 2 revealed clear evidence for resistivity anisotropy in the stress-free tetragonal state of underdoped $\text{BaFe}_{2-x}\text{Ni}_x\text{As}_2$ [Fig. 1(e)], these measurements cannot determine the sample detwinning ratio upon releasing

the uniaxial pressure at low temperature and microscopic origin of the resistivity anisotropy above T_s . To address these questions and compare the pressure dependence of the detwinning ratio with resistivity anisotropy, we carried out neutron diffraction experiments on BaFe_2As_2 using an *in situ* detwinning device similar to Fig. 1(b) and the flat-cone option of the IN8 triple-axis spectrometer at ILL [37]. In addition, we performed neutron Larmor diffraction measurement on $\text{BaFe}_{1.97}\text{Ni}_{0.03}\text{As}_2$ using the TRISP spectrometer [27–30]. We first describe neutron diffraction experiments on IN8 designed to study the detwinning ratio and its temperature dependence in strained and stress-free BaFe_2As_2 , as these results will allow us to determine whether the detwinning ratio is maintained after releasing the uniaxial strain below T_N . For the experiment, an annealed square-shaped single crystal of BaFe_2As_2 (~ 220 mg) was mounted on a specially designed sample stick inside an orange cryostat. The momentum transfer \mathbf{Q} in three-dimensional reciprocal space in \AA^{-1} is defined as $\mathbf{Q} = H\mathbf{a}^* + K\mathbf{b}^* + L\mathbf{c}^*$, where H , K , and L are Miller indices and $\mathbf{a}^* = \hat{\mathbf{a}}2\pi/a$, $\mathbf{b}^* = \hat{\mathbf{b}}2\pi/b$, $\mathbf{c}^* = \hat{\mathbf{c}}2\pi/c$ [12]. In the AF-ordered state of a 100% detwinned sample, the AF Bragg peaks should occur at $(\pm 1, 0, L)$ ($L = 1, 3, 5, \dots$) positions in reciprocal space and be absent at $(0, \pm 1, L)$. Our sample is aligned in the $[H, 0, L]$ scattering plane. Using the flat-cone setup on IN8 [37], we can access both $(1, 0, 5)$ and $(0, 1, 5)$ Bragg positions. When a pressure of ~ 24 MPa is applied along the b direction of BaFe_2As_2 , the sample is 100% detwinned with no magnetic scattering at $(0, 1, 5)$ [Figs. 3(a) and 3(b)]. After releasing the uniaxial pressure at 10 K, we see that the sample becomes partially twinned again with magnetic scattering intensity at both $I(1, 0, 5)$ and $I(0, 1, 5)$, giving a detwinning ratio of $\eta \approx 56\%$ ($\approx [I(1, 0, 5) - I(0, 1, 5)]/[I(1, 0, 5) + I(0, 1, 5)]$). This is consistent with transport measurements indicating a smaller resistivity anisotropy in the stress-free BaFe_2As_2 in the AF-ordered state [Fig. 2(f)]. Figure 3(c) shows temperature dependence of the magnetic scattering at $(1, 0, 5)$ and $(0, 1, 5)$ under 25 MPa uniaxial pressure and stress free. While the sample is 100% detwinned under 25 MPa below T_N with no magnetic scattering at $(0, 1, 5)$, the stress-free sample has finite intensity at both $(1, 0, 5)$ and $(0, 1, 5)$ below T_N . Figure 3(d) shows temperature dependence of η , which reveals a decreasing detwinning ratio on warming to T_N . For comparison, we also plot temperature dependence of the resistivity anisotropy, defined as $2(\rho_b - \rho_a)/(\rho_b + \rho_a)$, for the stress-free BaFe_2As_2 in Fig. 3(d). It is clear that temperature dependence of the resistivity anisotropy in the stress-free AF-ordered state of BaFe_2As_2 is approximately associated with the detwinning ratio.

In previous studies of the neutron extinction effect on the $(2, -2, 0)$ nuclear Bragg peak of BaFe_2As_2 in zero pressure [20], its intensity is found to deviate from normal behavior below ~ 150 K before displaying a steplike feature at $T_N \approx T_s \approx 138$ K, suggesting the presence of fluctuating orthorhombic structural domains above T_s . Using neutron Larmor diffraction with polarized neutrons, we can precisely determine temperature dependence of the lattice parameter and its distortion [27,29]. In a conventional diffraction experiment, a Bragg peak is observed when momentum transfer of neutrons ($|\mathbf{Q}| = |\mathbf{k}_i - \mathbf{k}_f| = 2k \sin \theta_B$, where the incident \mathbf{k}_i and outgoing wave vectors \mathbf{k}_f are equal in magnitude $|\mathbf{k}_i| = |\mathbf{k}_f| = k$) is equal to reciprocal lattice vector $|\mathbf{Q}| =$

$|\mathbf{G}(H, K, L)|$, where $|\mathbf{G}(H, K, L)| = 2\pi/d$ and d is the distance between two adjacent parallel plane of the lattice. The width of the Bragg peak in reciprocal space would provide a measure of the d -spacing distribution Δd . Unfortunately, temperature dependence of the lattice distortion in iron pnictides is too small to be seen in conventional diffraction experiments.

Larmor diffraction with polarized neutrons is capable of measuring lattice d spacing and its distribution Δd with a resolution better than 10^{-5} in $\Delta d/d$ [28,29]. The basic principle of neutron Larmor diffraction is shown in Fig. 4(a). We assume that a neutron polarized along the y direction with a velocity v_1 enters the first arm of neutron spin echo spectrometer with a constant magnetic field \mathbf{B} along the z direction and length L_1 . The diffracted neutron leaves the sample with velocity v_2 and enters the second arm with a \mathbf{B} along the z direction and length L_2 . Since neutron spin precession directions are tuned to be parallel with the diffraction planes in both L_1 and L_2 [see upper panel of Fig. 4(a)], the total neutron precession angle is $\phi_{\text{tot}} = 2\omega_L L/v$ for neutron diffraction measurement where $v = v_1 = v_2$, $L = L_1 = L_2$, and $\omega_L = \gamma|B|$ with $\gamma = 2\mu_N/\hbar = 2.916$ kHz/G being the gyromagnetic ratio of a neutron. When a Bragg condition is satisfied with $|\mathbf{Q}| = |\mathbf{G}(H, K, L)| = 2\pi/d = 2k \sin \theta_B$ and neutron velocity $v = \hbar k/m$, the total Larmor phase ϕ_{tot} can be written as $\phi_{\text{tot}} = 2\omega_L L m d \sin \theta_B / (\pi \hbar)$. Consequently, the variation of the Larmor phase is proportional to the change of the d spacing, or $\Delta\phi = \phi_{\text{tot}} \Delta d/d$. Therefore, by measuring the total Larmor phase ϕ_{tot} and its variation $\Delta\phi$, one can precisely determine the evolution of the lattice spacings and their distortion at different temperatures [Fig. 4(b)] [30].

Since transport measurements in Fig. 2 suggest that the resistivity anisotropy in the stress-free detwinned sample reduces dramatically above T_N and shows no visible anomaly across T_s for lightly electron-doped $\text{BaFe}_{2-x}\text{Ni}_x\text{As}_2$ [Figs. 2(g) and 2(h)], we decided to study temperature dependence of the lattice distortions and orthorhombicity $\delta = (a - b)/(a + b)$ in $\text{BaFe}_{1.97}\text{Ni}_{0.03}\text{As}_2$ [7], where T_s and T_N are well separated as determined from transport and neutron diffraction experiments. For this purpose, we focus on the $(4, 0, 0)$ Bragg peak, which has a d spacing $d = a/4$. In a classical second-order magnetic phase transition, one would expect that spin-spin correlation length increases upon cooling and diverges at T_N , while the underlying lattice correlations ξ remain long ranged and temperature independent. Surprisingly, our neutron Larmor diffraction measurements on strain-free $\text{BaFe}_{1.97}\text{Ni}_{0.03}\text{As}_2$ reveal that the lattice distortion ($\Delta d/d$) of the system shows no visible anomaly across T_s (≈ 118 K), but increases continuously upon cooling below T_s before collapsing abruptly below T_N (≈ 109 K) [Fig. 4(c)]. The increase in lattice distortion with decreasing temperature suggests a reduced lattice correlation length ξ upon cooling. Assuming that the d -spacing spread follows a Gaussian distribution, the Fourier transform of the Bragg peak width gives the lattice correlation length. For typical triple-axis experiments, the instrument resolution is about 300 \AA . With neutron Larmor diffraction, we find that the lattice correlation length ξ decreases upon cooling, changing smoothly from 2500 \AA around ~ 150 K to 1000 \AA just above T_N with no anomaly across T_s [Fig. 4(d)]. Figure 4(e) compares temperature dependence of the lattice orthorhombicity δ for $\text{BaFe}_{1.97}\text{Ni}_{0.03}\text{As}_2$ without applying external pressure and

in the stress-free situation. In both cases, we see that AF order induces a large change in lattice orthorhombicity, consistent with previous x-ray scattering work [7]. Therefore, $\text{BaFe}_{1.97}\text{Ni}_{0.03}\text{As}_2$ exhibits a strong magnetoelastic coupling near T_N .

Figure 5 summarizes temperature dependence of the resistivity anisotropy for uniaxial-strained and stress-free $\text{BaFe}_{2-x}\text{Ni}_x\text{As}_2$ with $x = 0, 0.015, 0.03, 0.05$. Similarly to previous work [16–18], we find that temperature dependence of the resistivity anisotropy in uniaxial-strained samples can be well described by a Curie-Weiss functional form above the strain free T_s and below T^* [see solid lines in Figs. 5(a)–5(d)]. When uniaxial strain is released, the resistivity anisotropy and its appearance temperature T^{**} are dramatically reduced. Nevertheless, it is clearly present above T_s in the tetragonal phase. For strain-free samples cooled from the high-temperature paramagnetic tetragonal phase, there is no resistivity anisotropy above T_s [see green data points in Fig. 5(a)], and the small resistivity anisotropy below T_N is due to slight imbalance in the twin domain populations.

To understand the observed resistivity anisotropy behavior, we consider a microscopic scenario as shown in Figs. 5(e)–5(h). In the low-temperature uniaxial-strained detwinned state, the undoped and underdoped $\text{BaFe}_{2-x}\text{Ni}_x\text{As}_2$ form a single-domain homogeneous magnetic ordered state with intrinsic resistivity anisotropy that is weakly electron-doping dependent [Figs. 5(a)–5(d), $\rho_b > \rho_a$]. Upon releasing the uniaxial strain, the sample becomes a partially detwinned AF-ordered state with reduced resistivity anisotropy [Fig. 5(f)]. Upon further warming to temperatures above T_N and T_s , these materials exhibit a large lattice distortion across T_N but much less anomaly across T_s [Figs. 4(c) and 4(d)]. These results suggest that the resistivity anisotropy seen in the narrow temperature region above T_s is due to the remnant local lattice distortions arising from the large magnetoelastic coupling across T_N [Fig. 5(g)]. The system finally relaxes to the true homogeneous tetragonal state without resistivity anisotropy at temperatures above T^{**} [Fig. 5(h)]. Since our neutron Larmor diffraction measurements showed no additional anomaly in lattice parameters and lattice distortion above T_s , we conclude that there is no thermodynamic phase transition at T^* and T^{**} in agreement with recent heat capacity measurements [21]. The resistivity anisotropy seen in the stress-free detwinned samples below T^{**} upon warming across T_N is then due to local spin nematic correlations and associated lattice distortions arising from the magnetoelastic coupling through the collinear AF state below T_N . The absence of such effect in the strain-free sample upon cooling confirms this scenario and the weakly first-order nature of the magnetic transition.

Having established a microscopic scenario for the observed resistivity anisotropy in the stress-free tetragonal state of $\text{BaFe}_{2-x}\text{Ni}_x\text{As}_2$ below T^{**} , it would be interesting to determine quantitatively the effect of uniaxial pressure on resistivity anisotropy below and above T_N and T_s . Figure 6 summarizes the uniaxial pressure dependence of the detwinning ratio and resistivity anisotropy for BaFe_2As_2 at different temperatures. In the AF-ordered state at 90 K, where neutron scattering results reveal a fully (100%) detwinned state for pressure above ~ 20 MPa, the resistivity anisotropy initially increases with increasing uniaxial pressure and detwinning

ratio, but does not saturate until ~ 70 MPa [Fig. 6(a)]. In the paramagnetic tetragonal state, previous work has shown that the resistivity anisotropy is proportional to the applied pressure at low pressure ($\ll 10$ MPa) [15–18]. We find that this is indeed the case at 150 K for pressure up to ~ 90 MPa [Fig. 6(b)]. The linear pressure dependence of the resistivity anisotropy at 150 K gradually changes upon cooling to the AF ordered state, and saturates to larger values with decreasing temperature [Fig. 6(b)]. This means that even in the fully detwinned AF ordered state, uniaxial pressure can affect the resistivity anisotropy of the system. Figure 6(c) shows pressure dependence of the normalized resistivity ρ_a and ρ_b . Upon reaching the fully detwinned state around 20 MPa, both ρ_a and ρ_b decrease linearly with increasing pressure, and show no saturation up to ~ 90 MPa [Fig. 6(c)]. This means that both expanding the lattice along the a axis and compressing the lattice along the b axis reduce resistivity.

Figure 6(d) shows the pressure dependence of the resistivity anisotropy at different temperatures below and above T_N and T_s for $\text{BaFe}_{1.985}\text{Ni}_{0.015}\text{As}_2$. Clear hysteresis is seen in the data, suggesting a partially detwinned sample after releasing the pressure. For the pressure-released partially detwinned sample, the resistivity anisotropy and the detwinning ratio follow the same trend below T_N , as shown in Fig. 6(a), which suggests the proximate association of the resistivity anisotropy with detwinning ratio η .

III. SUMMARY AND CONCLUSIONS

In summary, by using a specially designed *in situ* detwinning device, we have discovered the presence of resistivity anisotropy in the tetragonal phase of stress-free $\text{BaFe}_{2-x}\text{Ni}_x\text{As}_2$ below T^{**} , a temperature much lower than T^* associated with resistivity anisotropy in uniaxial-strained sample [13–16]. Our neutron diffraction experiments confirm the partially detwinned state in the stress-free sample, thus indicating that the observed resistivity anisotropy arises from local spin nematic correlations and lattice distortions. Furthermore, our neutron Larmor diffraction experiments on lightly electron-doped $\text{BaFe}_{1.97}\text{Ni}_{0.03}\text{As}_2$ indicate lattice distortions across T_N and T_s with no evidence of another phase transition above T_s . The uniaxial pressure necessary to detwin the sample can also affect the resistivity anisotropy both below and above T_N and T_s . In the paramagnetic state, the resistivity anisotropy is proportional to the applied uniaxial pressure up to ~ 90 MPa. In the fully detwinned AF-ordered state, both ρ_a and ρ_b decrease with increasing pressure. These results indicate that resistivity anisotropy in the stress-free tetragonal phase arises from the magnetoelastic coupling associated with static AF order, suggesting the presence of local Ising-nematic spin correlations and lattice distortions in the tetragonal state of iron pnictides near T_N . In the homogeneous paramagnetic tetragonal state, the presence of resistivity anisotropy is entirely induced by the applied uniaxial pressure. These results thus suggest that the C_4 rotational symmetry breaking spin excitations [20] and orbital ordering [24,25] in $\text{BaFe}_{2-x}\text{Ni}_x\text{As}_2$ above the strain free T_N and T_s are due to the externally applied uniaxial pressure necessary to detwin the sample below T_N via an enhanced nematic susceptibility in the undoped and underdoped regime.

ACKNOWLEDGMENTS

We are grateful to Sebastien Turc, E. Bourgeat-Lami, and E. Lelièvre-Berna of ILL, France, for designing and constructing the detwinning device used at IN8. The transport and neutron work at Rice is supported by the US NSF-DMR-1362219 and DMR-1436006 (P.D.). This work is also supported by the Robert A. Welch Foundation, Grants No. C-1839 (P.D.) and No. C-1411 (Q.S.). Q.S. is supported by the US NSF-DMR-1309531. The work at IOP, CAS in China is supported by the NSFC Program (No. 11374011) and CAS (SPRP-B: XDB07020300).

APPENDIX

The $\text{BaFe}_{2-x}\text{Ni}_{1-x}\text{As}_2$ single crystals were grown using the self-flux method as described before [38]. The crystal orientation was determined by the x-ray Laue machine, and the square-shaped samples were cut for Montgomery method resistivity measurements. The samples were annealed at 800 K for 2 days to reduce defects and disorder.

For sheetlike samples, measurement of anisotropic in-plane resistivity can be carried out by the Montgomery method [35,36]. The samples are cut along the a and b axis directions into a squared shape with the c axis perpendicular to the squared surface. Current is applied through contacts at two adjacent corners of the planar face and the potential is measured at the other two corners at the same plane [Fig. 7(a)]. From the measurements, we can get $R_a = (V^+ - V^-)/I_1$. Similar measurements can be done with the electrical connections rotated 90° with respect to the original setup, which gives $R_b = (V^+ - V^-)/I_2$ [Fig. 7(b)]. This will allow calculations of the resistivity anisotropy.

Results from an anisotropic sample with dimensions l_1, l_2, l_3 , and resistivity ρ_1, ρ_2, ρ_3 can be estimated from an isotropic sample with dimension l'_1, l'_2, l'_3 with the transformation

$$\rho^3 = \rho_1 \rho_2 \rho_3 \quad (\text{A1})$$

and

$$l'_i = l_i(\rho_i/\rho)^{1/2}. \quad (\text{A2})$$

Through theoretical calculations, we can get for small l_1/l_2 ratio

$$\frac{l'_2}{l'_1} \simeq \frac{1}{2} \left[\frac{1}{\pi} \ln \frac{R_b}{R_a} + \sqrt{\left[\frac{1}{\pi} \ln \frac{R_b}{R_a} \right]^2 + 4} \right] \quad (\text{A3})$$

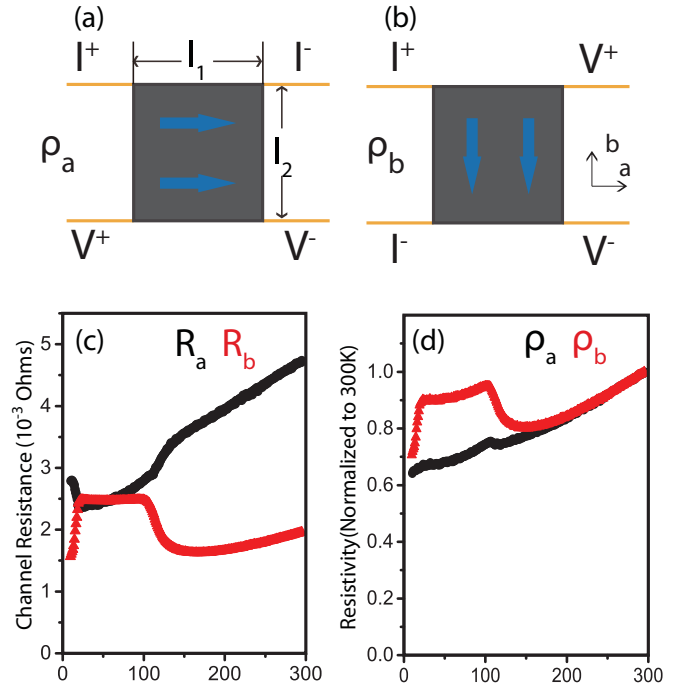


FIG. 7. (Color online) Schematic diagram of Montgomery method, wire connections, current flow direction, and sample dimensions. (a), (b) Schematic illustration of Montgomery method: wire connections and current flow directions. Sample plane dimensions are $l_1 \times l_2$. The blue arrows on the sample are the current direction for each setup. (c) Resistance data of $\text{BaFe}_{1.97}\text{Ni}_{0.03}\text{As}_2$ from the two channels on the PPMS resistivity puck. Black and red indicate the direction of the resistance measured on the channel. (d) Normalized resistivity calculated from (c).

and the anisotropic resistivity in the plane can be written as

$$\rho_1 = A(l'_1/l'_2)R_a \sinh[\pi l'_2/l'_1] \quad (\text{A4})$$

and

$$\rho_2 = B(l'_2/l'_1)R_b \sinh[\pi l'_1/l'_2]. \quad (\text{A5})$$

In the case of $\text{BaFe}_{2-x}\text{Ni}_x\text{As}_2$, A and B are prefactors that can be normalized as $\rho_1(300 \text{ K}) = \rho_2(300 \text{ K})$. Then ρ_1 and ρ_2 can be determined by resistance measurements R_a and R_b by two different channels on the PPMS resistivity puck, as shown in Figs. 7(c) and 7(d). ρ_1 and ρ_2 derived from the Montgomery method are the equivalent resistivity by the mixture of two domains angling 90° with initial resistivity of ρ_{a0} and ρ_{b0} .

- [1] E. Fradkin, S. A. Kivelson, M. J. Lawler, J. P. Eisenstein, and A. P. Mackenzie, Nematic Fermi fluids in condensed matter physics, *Annu. Rev. Condens. Matter Phys.* **1**, 153 (2010).
- [2] Y. Kamihara, T. Watanabe, M. Hirano, and H. Hosono, Iron-based layered superconductor $\text{La}[\text{O}_{1-x}\text{F}_x]\text{FeAs}$ ($x = 0.05\text{--}0.12$) with $T_c = 26 \text{ K}$, *J. Am. Chem. Soc.* **130**, 3296 (2008).

- [3] G. R. Stewart, Superconductivity in iron compounds, *Rev. Mod. Phys.* **83**, 1589 (2011).
- [4] P. C. Dai, Antiferromagnetic order and spin dynamics in iron-based superconductors, *Rev. Mod. Phys.* **87**, 855 (2015).
- [5] C. de la Cruz, Q. Huang, J. W. Lynn, Jiying Li, W. Ratcliff, II, J. L. Zarestky, H. A. Mook, G. F. Chen, J. L. Luo, N. L. Wang, and P. C. Dai, Magnetic order close to superconductivity in the

- iron-based layered $\text{LaO}_{1-x}\text{F}_x\text{FeAs}$ systems, *Nature (London)* **453**, 899 (2008).
- [6] Q. Huang, Y. Qiu, Wei Bao, M. A. Green, J. W. Lynn, Y. C. Gasparovic, T. Wu, G. Wu, and X. H. Chen, Neutron-Diffraction Measurements of Magnetic Order and a Structural Transition in the Parent BaFe_2As_2 Compound of FeAs-Based High-Temperature Superconductors, *Phys. Rev. Lett.* **101**, 257003 (2008).
- [7] M. G. Kim, R. M. Fernandes, A. Kreyssig, J. W. Kim, A. Thaler, S. L. Bud'ko, P. C. Canfield, R. J. McQueeney, J. Schmalian, and A. I. Goldman, Character of the structural and magnetic phase transitions in the parent and electron-doped BaFe_2As_2 compounds, *Phys. Rev. B* **83**, 134522 (2011).
- [8] C. Lester, J.-H. Chu, J. G. Analytis, S. C. Capelli, A. S. Erickson, C. L. Condon, M. F. Toney, I. R. Fisher, and S. M. Hayden, Neutron scattering study of the interplay between structure and magnetism in $\text{Ba}(\text{Fe}_{1-x}\text{Co}_x)_2\text{As}_2$, *Phys. Rev. B* **79**, 144523 (2009).
- [9] S. Nandi, M. G. Kim, A. Kreyssig, R. M. Fernandes, D. K. Pratt, A. Thaler, N. Ni, S. L. Bud'ko, P. C. Canfield, J. Schmalian, R. J. McQueeney, and A. I. Goldman, Anomalous Suppression of the Orthorhombic Lattice Distortion in Superconducting $\text{Ba}(\text{Fe}_{1-x}\text{Co}_x)_2\text{As}_2$ Single Crystals, *Phys. Rev. Lett.* **104**, 057006 (2010).
- [10] M. Yoshizawa, D. Kimura, T. Chiba, S. Simayi, Y. Nakanishi, K. Kihou, C.-H. Lee, A. Iyo, H. Eisaki, M. Nakajima, and S. Uchida, Structural quantum criticality and superconductivity in iron-based superconductor $\text{Ba}(\text{Fe}_{1-x}\text{Co}_x)_2\text{As}_2$, *J. Phys. Soc. Jpn.* **81**, 024604 (2012).
- [11] H. Q. Luo, R. Zhang, M. Laver, Z. Yamani, M. Wang, X. Y. Lu, M. Y. Wang, Y. C. Chen, S. L. Li, S. Chang, J. W. Lynn, and P. C. Dai, Coexistence and Competition of the Short-Range Incommensurate Antiferromagnetic Order with the Superconducting State of $\text{BaFe}_{2-x}\text{Ni}_x\text{As}_2$, *Phys. Rev. Lett.* **108**, 247002 (2012).
- [12] X. Y. Lu, H. Gretarsson, R. Zhang, X. Liu, H. Q. Luo, W. Tian, M. Laver, Z. Yamani, Y.-J. Kim, A. H. Nevidomskyy, Q. Si, and P. C. Dai, Avoided Quantum Criticality and Magnetoelastic Coupling in $\text{BaFe}_{2-x}\text{Ni}_x\text{As}_2$, *Phys. Rev. Lett.* **110**, 257001 (2013).
- [13] J. H. Chu, J. G. Analytis, K. De Greve, P. L. McMahon, Z. Islam, Y. Yamamoto, and I. R. Fisher, In-plane resistivity anisotropy in an underdoped iron arsenide superconductor, *Science* **329**, 824 (2010).
- [14] M. A. Tanatar, E. C. Blomberg, A. Kreyssig, M. G. Kim, N. Ni, A. Thaler, S. L. Bud'ko, P. C. Canfield, A. I. Goldman, I. I. Mazin, and R. Prozorov, Uniaxial-strain mechanical detwinning of CaFe_2As_2 and BaFe_2As_2 crystals: Optical and transport study, *Phys. Rev. B* **81**, 184508 (2010).
- [15] I. R. Fisher, L. Degiorgi, and Z. X. Shen, In-plane electronic anisotropy of underdoped '122' Fe-arsenide superconductors revealed by measurements of detwinned single crystals, *Rep. Prog. Phys.* **74**, 124506 (2011).
- [16] J. H. Chu, H.-H. Kuo, J. G. Analytis, I. R. Fisher, Divergent nematic susceptibility in an iron arsenide superconductor, *Science* **337**, 710 (2012).
- [17] H.-H. Kuo, M. C. Shapiro, S. C. Riggs, and I. R. Fisher, Measurement of the elastoresistivity coefficients of the underdoped iron arsenide $\text{Ba}(\text{Fe}_{0.975}\text{Co}_{0.025})_2\text{As}_2$, *Phys. Rev. B* **88**, 085113 (2013).
- [18] H.-H. Kuo, J.-H. Chu, S. A. Kivelson, and I. R. Fisher, Ubiquitous signatures of nematic quantum criticality in optimally doped Fe-based superconductors, [arXiv:1503.00402](https://arxiv.org/abs/1503.00402).
- [19] C. Dhital, T. Hogan, Z. Yamani, R. J. Birgeneau, W. Tian, M. Matsuda, A. S. Sefat, Z. Wang, and S. D. Wilson, Evolution of antiferromagnetic susceptibility under uniaxial pressure in $\text{Ba}(\text{Fe}_{1-x}\text{Co}_x)_2\text{As}_2$, *Phys. Rev. B* **89**, 214404 (2014).
- [20] X. Y. Lu, J. T. Park, R. Zhang, H. Q. Luo, A. H. Nevidomskyy, Q. Si, and P. C. Dai, Nematic spin correlations in the tetragonal state of uniaxial-strained $\text{BaFe}_{2-x}\text{Ni}_x\text{As}_2$, *Science* **345**, 657 (2014).
- [21] X. Luo, V. Stanev, B. Shen, L. Fang, X. S. Ling, R. Osborn, S. Rosenkranz, T. M. Benseman, R. Divan, W.-K. Kwok, and U. Welp, Antiferromagnetic and nematic phase transitions in $\text{BaFe}_2(\text{As}_{1-x}\text{P}_x)_2$ studied by ac microcalorimetry and SQUID magnetometry, *Phys. Rev. B* **91**, 094512 (2015).
- [22] S. Kasahara, H. J. Shi, K. Hashimoto, S. Tonegawa, Y. Mizukami, T. Shibauchi, K. Sugimoto, T. Fukuda, T. Terashima, A. H. Nevidomskyy, and Y. Matsuda, Electronic nematicity above the structural and superconducting transition in $\text{BaFe}_2(\text{As}_{1-x}\text{P}_x)_2$, *Nature (London)* **486**, 382 (2012).
- [23] R. M. Fernandes, A. V. Chubukov, and J. Schmalian, What drives nematic order in iron-based superconductors?, *Nat. Phys.* **10**, 97 (2014).
- [24] M. Yi, D. H. Lu, J. H. Chu, J. G. Analytis, A. P. Sorini, A. F. Kemper, B. Moritz, R. G. Moore, M. Hashimoto, W. S. Lee, Z. Hussain, T. P. Devereaux, I. R. Fisher, and Z. X. Shen, Symmetry-breaking orbital anisotropy observed for detwinned $\text{Ba}(\text{Fe}_{1-x}\text{Co}_x)_2\text{As}_2$ above the spin density wave transition, *Proc. Natl. Acad. Sci. USA* **108**, 6878 (2011).
- [25] Y. Zhang, C. He, Z. R. Ye, J. Jiang, F. Chen, M. Xu, Q. Q. Ge, B. P. Xie, J. Wei, M. Aeschlimann, X. Y. Cui, M. Shi, J. P. Hu, and D. L. Feng, Symmetry breaking via orbital-dependent reconstruction of electronic structure in detwinned NaFeAs , *Phys. Rev. B* **85**, 085121 (2012).
- [26] C. Mirri, A. Dusza, S. Bastelberger, J.-H. Chu, H.-H. Kuo, I. R. Fisher, and L. Degiorgi, Hysteretic behavior in the optical response of the underdoped Fe arsenide $\text{Ba}(\text{Fe}_{1-x}\text{Co}_x)_2\text{As}_2$ in the electronic nematic phase, *Phys. Rev. B* **89**, 060501(R) (2014).
- [27] M. T. Rekveldt, T. Keller, and R. Golub, Larmor precession, a technique for high-sensitivity neutron diffraction, *Europhys. Lett.* **54**, 342 (2001).
- [28] S. P. Bayrakci, T. Keller, K. Habicht, and B. Keimer, Spin-wave lifetimes throughout the Brillouin zone, *Science* **312**, 1926 (2006).
- [29] C. Pfleiderer, P. Böni, T. Keller, U. K. Rößler, and A. Rosch, Non-Fermi liquid metal without quantum criticality, *Science* **316**, 1871 (2007).
- [30] X. Y. Lu, T. Keller, W. L. Zhang, Y. Song, J. T. Park, H. Q. Luo, S. L. Li, and P. C. Dai, Effect of uniaxial pressure on structural and magnetic phase transitions in electron-doped $\text{BaFe}_{2-x}\text{Ni}_x\text{As}_2$ superconductors, [arXiv:1507.04191](https://arxiv.org/abs/1507.04191).
- [31] R. M. Fernandes, A. E. Böhmer, C. Meingast, and J. Schmalian, Scaling between Magnetic and Lattice Fluctuations in Iron Pnictide Superconductors, *Phys. Rev. Lett.* **111**, 137001 (2013).
- [32] P. Chandra, P. Coleman, and A. I. Larkin, Ising Transition in Frustrated Heisenberg Models, *Phys. Rev. Lett.* **64**, 88 (1990).

- [33] J. Dai, Q. Si, J. X. Zhu, and E. Abrahams, Iron pnictides as a new setting for quantum criticality, *Proc. Natl. Acad. Sci. USA* **106**, 4118 (2009).
- [34] J. P. Hu and C. K. Xu, Nematic orders in iron-based superconductors, *Physica C* **481**, 215 (2012).
- [35] H. C. Montgomery, Method for measuring electrical resistivity of anisotropic materials, *J. Appl. Phys.* **42**, 2971 (1971).
- [36] C. A. M. dos Santos, A. de Campos, M. S. da Luz, B. D. White, J. J. Neumeier, B. S. de Lima, and C. Y. Shigue, Procedure for measuring electrical resistivity of anisotropic materials: A revision of the Montgomery method, *J. Appl. Phys.* **110**, 083703 (2011).
- [37] M. Kempa, B. Janousova, J. Saroun, P. Flores, M. Boehm, F. Demmel, and J. Kulda, The FlatCone multianalyzer setup for ILL's three-axis spectrometers, *Physica B* **385-386**, 1080 (2006).
- [38] Y. C. Chen, X. Y. Lu, M. Wang, H. Q. Luo, and S. L. Li, Systematic growth of $\text{BaFe}_{2-x}\text{Ni}_x\text{As}_2$ large crystals, *Supercond. Sci. Technol.* **24**, 065004 (2011).